Phase Diagrams of Microemulsions containing Reducing Agents and Metal Salts as Bases for the Synthesis of Metallic Nanoparticles

Reza Najjar*[1], Cosima Stubenrauch[2]

[1] *Faculty of Chemistry, University of Tabriz, 29 Bahman Blvd. Tabriz, Iran*

[2] *School of Chemical and Bioprocess Engineering, Centre for Synthesis and Chemical Biology (CSCB), SFI-Strategic Research Cluster in Solar Energy Conversion, University College Dublin, Belfield, Dublin 4, Ireland*

ABSTRACT

We studied the phase diagrams of microemulsions with a view to using these systems for the synthesis of metallic Pt, Pb, and Bi nanoparticles as well as of intermetallic Pt/Pb and Pt/Bi nanoparticles. The microemulsions consisted of H_2O/salt – *n*-decane – SDS – 1-butanol. The salt was either one metal precursor ($H_2PtCl_6 \cdot 6H_2O$, $Pb(NO_3)_2$, or $Bi(NO_3)_3 \cdot 5H_2O$), a mixture of two metal precursors ($H_2PtCl_6 \cdot 6H_2O$ + $Pb(NO_3)_2$ or $H_2PtCl_6 \cdot 6H_2O$ + $Bi(NO_3)_3 \cdot 5H_2O$), or the reducing agent ($NaBH_4$). In addition, other salts needed to be added in order to solubilize the metal precursors, to stabilize the reducing agent, and to adjust the ionic strength. Combining the microemulsion (μe1) that contains the metal precursor(s) with the microemulsion (μe2) that contains the reducing agent leads to metallic nanoparticles. To study systematically how the shape and size of the synthesized metallic nanoparticles depend on the size and shape of the respective microemulsion droplets, first of all one has to find those conditions under which μe1 and μe2 have the same structure. For that purpose we determined the water emulsification failure boundary (*wefb*) of each microemulsion as it is at the *wefb* where the water droplets are known to be spherical. We found that the ionic strength (*I*) of the aqueous phase as well as the hard acid and hard base properties of the ions are the key tuning parameters for the location of the *wefb*.

Keywords: water emulsification failure boundary, w/o-microemulsions, nanoreactors, metallic nanoparticles

1. Introduction

Fuel cells working at low temperatures with methanol or ethanol are of special interest because of their low production cost and easy availability. The anodic material of these fuel cells should have reasonable catalytic properties for the oxidation of the related alcohols. Platinum is one of the materials used for this purpose [1,2]. However, apart from the high price, its catalytic activity decreases dramatically over time. This is because of the adsorption of oxidation products such as CO, $COH^{\cdot}$, $OH^{\cdot}$ on the catalyst sites causing permanent blockage. The costs can be reduced by using Pt nano-crystallites deposited on less expensive materials (such as vitreous carbon) but still the poisoning of the catalyst is an issue [1]. Another way to overcome this problem is to modify Pt by adding other elements such as Sn, Bi or Pb, *i.e.* by synthesizing intermetallic phases (alloys). This has proved to be a solution to the problem as it prevents the fast poisoning of the catalyst [1, 3-10]. Different mechanisms were suggested for the role of the added modifying element, namely (a) adsorption of the alcohol molecules on Pt and oxygen derivatives generated from the decomposition of water on the added element (for example Pb, Sn) [11-13], (b) "ligand effect" (electronic interaction of the added element with Pt which changes the adsorption energy of the adsorbate on Pt) [14], and (c) homogeneous catalytic reactions which was confirmed by the presence of complexed cations of the added element in the reaction media [12,15]. Hence, because of their expected specific catalytic activities and selectivities, intermetallic (nano)particles synthesized by different techniques [16-19] are gaining in importance. For example, Abruna and co-workers [20,21] have prepared Pt/Pb intermetallic phases by heating metals to ca. 1000 °C under vacuum in a sealed quartz tube and used them as catalyst for fuel cells. Moreover, they have prepared Pt/Pb and Pt/Bi nanoparticles using solvochemical reduction techniques [22-25]. In both cases the resulting alloys have shown improved performance as electrocatalysts for the oxidation of small organic molecules compared to the pure Pt catalyst.

A simple technique for the synthesis of metallic nanoparticles under very mild reaction conditions (*e.g.* at room temperature) is the use of water-in-oil (w/o) microemulsions. Using microemulsions instead of the above mentioned solvochemical reduction techniques allows us to synthesize nanoparticles of low polydispersity and tuneable size [26-28]. Microemulsions are thermo-dynamically stable mixtures of at least three components, namely, water, oil, and a surfactant with domain sizes of 5 - 50 nm [29]. The domains can be discrete (water or oil droplets) or bicontinuous [30]. As it is known how to tune the structure and size of the domains, microemulsions are becoming increasingly important as micro-reactors and/or templates. Although w/o-microemulsions have been widely used to synthesize monometallic nanoparticles, the synthesis of intermetallic nanoparticles via w/o microemulsions is still a challenge and has been successful only in the case of

metals with similar reduction potentials (*e.g.* Pt/Ag [31], Pt/Au [32], Pt/Pd [33]). The synthesis of intermetallic nanoparticles of metals with largely different reduction potentials has not yet been achieved. The difficulties mainly arise from the need to "co-reduce" two metals with largely different redox potentials and from the low water stability of most reducing agents. As already mentioned Pt/Bi and Pt/Pb intermetallic compounds exhibit unique catalytic properties in fuel cell applications [20,24-27] compared to the catalytic activity of pure Pt. Thus introducing new routes towards the synthesis of intermetallic Pt/Bi and Pt/Pb nanoparticles ($[PtCl_6]^{2-}/[PtCl_4]^{2-}$ = +0.68V, $[PtCl_4]^{2-}$/Pt = +0.76V[1], Bi^{3+}/Bi = +0.22 V, and Pb^{2+}/Pb = -0.13 V) and testing their catalytic activity in fuel cells is of prime importance. Studying the phase behaviour of the microemulsions is a very important part of the work, which requires a careful determination of the water emulsification failure boundary (*wefb*) because it is at the *wefb* where discrete water droplets in a continuous oil phase are formed.

SANS, NMR self-diffusion, static and dynamic light scattering measurements performed along the oil emulsification failure boundary can be self-consistently interpreted in terms of spherical oil-swollen micelles, interacting through a hard sphere potential over a large concentration range. The presence of spherical micelles can be understood in terms of the flexible surface model where structure and stability are governed by the curvature and the elastic properties of the surfactant monolayer [30,35,36-37-39]. From extensive phase studies it is known that the oil and the water emulsification phase boundaries, respectively, play the same general role [30] – they are just located on different sides, namely the water- and the oil-rich side, of the phase diagram. Not surprisingly, SANS measurements at the water emulsification failure boundary can also be interpreted in terms of spherical water-swollen micelles interacting through a hard sphere potential [35,36,40]. A further proof of the spherical nature of water droplets at the *wefb* was obtained via transmission electron microscopy [41]. The diameter *d* of the spherical droplets at the *wefb* can be calculated according to

$$d = 6\delta \frac{\phi_{disp}}{\phi_{C,i} + \phi_{D,i}} \approx 6nm \frac{w_A + \gamma}{\gamma} \qquad \text{Eq. [1]}$$

[42] where $\delta \approx$ 1 nm is the thickness of the amphiphilic interfacial film, ϕ_{disp} is the volume fraction of the dispersed phase, and $\phi_{C,i}$ and $\phi_{D,i}$ are the volume fractions of the surfactant and co-surfactant forming the interface.

The final aim of our work is to synthesize intermetallic Pt-Bi and / or Pt-Pb nanoparticles via w/o-microemulsions. For this purpose first of all one has to find a suitable microemulsion system as well

[1] $H_2[PtCl_6]$ was found to be reduced from Pt^{4+} to Pt via Pt^{2+} [34].

as the experimental conditions under which w/o-microemulsions are formed. Secondly, the conditions for the co-reduction of two metal salts whose reduction potentials are quite different have to be specified. The starting point of our study was the model system H_2O/NaCl – *n*-decane – SDS – 1-butanol. First, the water emulsification failure boundary (*wefb*) of this system was determined. Based on this phase diagram, we studied the influence of (a) different types and amounts of electrolytes, (b) the reducing agent, and (c) different metal precursors on the location of the *wefb* to preserve the desired w/o-microemulsion structure. To our knowledge these extensive phase studies are usually not carried out and we only could find one detailed study of this kind [43]. Generally two microemulsions with a fixed water/surfactant ratio are prepared without taking into account the influence the added metal salt or the reducing agent has on the size and the structure of the dispersed water droplets. In our previous study we indeed adjusted changes of the phase boundaries caused by adding the different salts. However, we did not determine the location of the complete *wefb* but rather the location of one point on the *wefb* [28]. With the present study we want to fill this gap. Detailed phase diagrams will be presented and the influence of the different salts on the *wefb* will be discussed. Knowing the location of the complete *wefb* will allow us to efficiently use these microemulsions as reaction media for the synthesis of nanoparticles in following studies.

2. Experimental Part

Materials

The following chemicals were all used as received without any further purification: sodium chloride, NaCl (Merck, 99.5%), sodium borhydride, $NaBH_4$ (Sigma-Aldrich, 98%), sodium dodecyl sulfate, SDS (Sigma-Aldrich, 99.0%), chloroplatinic acid hexahydrate, $H_2PtCl_6 \cdot 6H_2O$ (Sigma-Aldrich, ACS reagent), lead(II) nitrate, $Pb(NO_3)_2$ (Aldrich, 99.999%), *n*-decane (Aldrich, 99%), bismuth(III) nitrate pentahydrate, $Bi(NO_3)_3 \cdot 5H_2O$ (Sigma, 99.999%), sodium hydroxide, NaOH (BDH, 99.999%), nitric acid, HNO_3 (BDH, 69.5%), sodium nitrate, $NaNO_3$ (Fluka, 99.99%), 1-butanol (Romil, 99.9%). Fresh milli-Q water was taken from a Millipore unit.

Determination of Phase Diagrams

Phase diagrams were measured using glass water basins comprising of an immersion thermostat, a magnetic stirrer, a light source, and a thermometer. The temperature of the basin was monitored with ±0.01 °C precision (thermometer model 1521, Hart Scientific). A halogen lamp was used as light source (Gerhardt Optic, Germany). For the determination of the phase diagrams, aqueous solutions containing metal precursors and reducing agent, respectively, were prepared. Afterwards the desired amounts of these solutions, *n*-decane, and SDS (sodium dodecylsulfate) were weighted

into test tubes, which were then sealed with stoppers. The test tubes were placed in the water basin at 21.0 °C and stirred for 5 minutes. While stirring 1-butanol was added and the resulting phase changes were monitored**.**

A, B, C, and D denote the aqueous phase (with or without electrolytes), oil, surfactant, and co-surfactant, respectively. The composition of the samples is given by the following definitions:

γ_b = mass fraction of surfactant in the oil phase

$$\gamma_b = \frac{m_C}{m_C + m_B}, \qquad \text{Eq. [2]}$$

w_A = total mass fraction of aqueous phase (with or without electrolytes)

$$w_A = \frac{m_A}{\sum_i m_i}, \qquad \text{Eq. [3]}$$

ε = mass fraction of dissolved inorganic salt in the aqueous phase

$$\varepsilon = \frac{m_{salt}}{m_{salts} + m_A}, \qquad \text{Eq. [4]}$$

and w_D = total mass fraction of co-surfactant

$$w_D = \frac{m_D}{\sum_i m_i}. \qquad \text{Eq. [5]}$$

3. Results

3.1. Phase Diagrams of the Base Microemulsion Systems

For the synthesis of nanoparticles via w/o-microemulsions the phase diagram of the respective microemulsion has to be measured to know the conditions and compositions at which water-in-oil droplets are formed. Possible ways of tuning the phase behavior – and thus the formation of w/o-microemulsions – are temperature changes, the addition of a co-surfactant, and changes of the salt content [44-47]. In the present study all measurements were carried out at constant temperature and

the amount of co-surfactant (1-butanol) was changed to locate the water emulsification failure boundary (*wefb*) of the microemulsion that contained the metal salt(s) and the reducing agent, respectively. The starting point for the study was the base system H_2O/salt – *n*-decane – SDS – 1-butanol [28] of which the *wefb* was measured as a function of the 1-butanol and the brine content keeping the temperature (T = 21°C), γ_b (see Eq.2), and ε (see Eq.4) constant. To understand how the type and the amount of salt influence the location of the *wefb*, the phase diagrams for two different electrolytes (NaCl and NaOH) were measured at two different electrolyte concentrations (ε = 0.01 and ε = 0.02). The results for NaCl are seen in Fig.1, while those for NaOH are seen in Fig.S1 of the Supporting Material.

Figure 1

Looking at Fig.1 (and Fig.S1) one sees that an increase in the electrolyte content leads to a shift of the *wefb* towards both lower water and lower 1-butanol contents. This trend is observed for both systems. Comparing the NaCl- (Fig.1) and the NaOH-, (Supporting Material, Fig.S1) containing systems at equal ε-values, one sees that the *wefb* of the latter is again slightly shifted towards lower water and 1-butanol contents. This shift can be explained by the fact that ε is measured in weight fractions and not in molar concentrations (note that equal weight fractions correspond to different molar concentrations, namely c(NaOH) > c(NaCl)). Thus one can conclude for a 1:1 electrolyte that the *wefb* is shifted towards lower water and 1-butanol contents with increasing molar concentration of the electrolyte. We will come back to this point in section 4.

3.2. Phase Diagrams of Microemulsions containing Reducing Agent

Having learnt how sensitive the location of the *wefb* is towards changes of the electrolyte content we characterized the microemulsions required for the synthesis of nanoparticles in detail. As we have chosen $NaBH_4$ as reducing agent for the metal salts we measured three phase diagrams of $NaBH_4$-containing system. In all cases NaOH was added as $NaBH_4$ has a better stability in basic solutions. Firstly, we studied the phase diagram of two $NaBH_4$/NaOH containing systems which are planned to be used for the synthesis of Pt nanoparticles. Secondly, we measured the phase diagram of a system containing $NaBH_4$/NaOH/$NaNO_3$ which is planned to be used for the synthesis of Bi, Pb, and the intermetallic nanoparticles. In the latter case $NaNO_3$ was added to adjust the salt content such that it equals the salt content of the microemulsions containing the metal precursors (see sections 3.3, 3.4, and section 4). The resulting phase diagrams are shown and discussed in the Supporting Material (Fig.S2) and the compositions of the aqueous phases are given in Tab.1.

Table 1

Similar results as for the base systems studied in section 3.1 have been observed (for more detail see Supporting Material. In all cases 1:1 electrolytes have been used and thus what was concluded in relation to Fig.1 still holds true: the *wefb* is shifted towards lower water and 1-butanol contents with increasing electrolyte content. We will come back to this point in section 4.

3.3. Phase Diagrams of Microemulsions containing one Metal Precursor

The next step was to study the phase diagrams of systems containing one metal precursor which will be needed for the synthesis of monometallic nanoparticles. We recall that the final goal is to combine two microemulsions the water droplets of which have the same size but different content: the droplets of one microemulsion (μe1) contain the metal precursor, while those of the other (μe2) contain the reducing agent. The easiest way to achieve this goal is to mix two systems of equal w_A and γ_b for which the location of the *wefb* is as similar as possible (*i.e.* the *wefb* is at 1-butanol concentrations as similar as possible). As was shown above, the salt content is an important tuning parameter for the location of the *wefb* and we found that equal ε-values do not lead to the same location of the *wefb*. We concluded in section 3.2 that the tuning parameter is the molar concentration. However, the situation becomes more complicated once the metal precursors are added. The metal salts are no 1:1 electrolytes and thus different ionic strengths also come into play. To our knowledge *wefb* measurements as a function of the ionic strength have not been published yet. Thus, without having any reference, we decided to study microemulsions with metal precursors at ε-values which are the same as those of the respective reducing microemulsions (see Supporting Material, Fig.S2). The resulting phase diagrams of three microemulsions containing different metal precursors are shown in Fig.2 and the compositions of the aqueous phases are given in Tab.2.

Figure 2

Table 2

(a) **H_2PtCl_6**: In Fig.2(a) the phase diagrams of a microemulsion containing the metal salt H_2PtCl_6 and the electrolyte NaCl (μe1) as well as that of the corresponding reducing microemulsion (μe2) are shown. Although the total electrolyte content in both systems is ε = 0.02, the two *wefbs* do not lie on top of each other. Part of this mismatch is again caused by

$_2PtCl_6$ is a 1:2 electrolyte as it dissociates into H^+ and $PtCl_6^{2-}$ and thus different ionic strengths also come into play, namely 0.23 M for µe1 and 0.51 M for µe2 (see Tab.1 and Tab.2). Whether it is the molar concentration of the ions or the ionic strength of the solution that should be considered as tuning parameter for the location of the *wefb* will be discussed in section 4.

(b) **$Bi(NO_3)_3$**: As bismuth (III) nitrate salt is only soluble in acid solutions we had to add 10 wt.-% HNO_3 (ε_{HNO3} = 0.10) to the aqueous phase of µe1. To adjust the electrolyte content of the respective µe2, we added 8 wt.-% $NaNO_3$ (ε_{NaNO3} = 0.08) to the aqueous phase and measured the *wefb* (see Supporting Material, Fig.S2(b)). As was the case for the Pt-salt, the two *wefb*s do not lie on top of each other although both systems contain the same weight fraction of electrolyte, namely ε = 0.11. However, as can be seen in Tab.1 and Tab.2, the difference can neither be explained by different molar concentrations nor by different ionic strengths. Although the molar concentration of µe1 is slightly lower than that of µe2, the upper phase boundary is located – other than expected – at lower water and 1-butanol contents, while the lower phase boundary is nearly unaffected. An explanation with the ionic strengths is not possible either as the ionic strengths of µe1 and µe2 are the same. In section 4, we will discuss a third possible tuning parameter, which may explain the different *wefb*s seen in Fig.2(b).

(c) **$Pb(NO_3)_2$**: In Fig.2(c) the phase diagrams of a microemulsion containing the metal salt $Pb(NO_3)_2$ and the electrolyte $NaNO_3$ (µe1) as well as that of the corresponding reducing microemulsion (µe2) are shown. Regarding the total electrolyte concentration we decided to use ε = 0.11 for all further studies as this seemed to be the lower limit for the Bi-salt. Accordingly, the reducing microemulsion of choice is the one with ε_{NaBH4} = 0.02, ε_{NaOH} = 0.01, and ε_{NaNO3} = 0.08. We used $NaNO_3$ and not NaCl to adjust the ε-values because insoluble $PbCl_2$ would form and precipitate. Comparing the phase diagrams of µe1 and µe2 one sees again that two *wefb*s do not match. As was the case for the Pt-salt, the difference can be explained by the larger molar concentration and the larger ionic strength of the reducing microemulsion (see Tab.1 and Tab.2).

3.4. Phase Diagrams of Microemulsions containing two Metal Precursors

For the preparation of intermetallic nanoparticles a microemulsion which contains both metal salts will be required. Hence, microemulsions with two metal salts were prepared and their phase diagrams were measured. As a first approach equal weight fractions of the two different metal salts were used[2]. The resulting phase diagrams are shown in Fig.3 and the compositions of the aqueous phases are given in Tab.2.

Figure 3

(a) **H_2PtCl_6 and $Bi(NO_3)_3$**: Comparing Fig.3(a) with Fig.2(b), one sees that exchanging half of $Bi(NO_3)_3$ by H_2PtCl_6 does not change the phase boundaries significantly. As was the case for the pure $Bi(NO_3)_3$, the observed trend can neither be explained by different molar concentrations nor by different ionic strengths, which are both slightly lower in μe1 compared to μe2. We will discuss in section 4 that a lower molar concentration and a lower ionic strength should lead to an opposite shift of the phase boundaries, which, in turn, motivated us to think about a third possible tuning parameter.

(b) **H_2PtCl_6 and $Pb(NO_3)_2$**: Comparing Fig.3(b) with Fig.2(c), one sees that exchanging half of $Pb(NO_3)_2$ by H_2PtCl_6 does not change the phase boundaries significantly. As was the case for the pure $Pb(NO_3)_3$, the observed trend can be explained by different molar concentrations and different ionic strengths, which are both lower in μe1 compared to μe2. We will come back to this point in section 4.

4. Discussion

Regarding the phase diagrams of microemulsions it is well known that discrete water droplets in a continuous oil phase are formed at the water emulsification failure boundary (*wefb*). Thus it is necessary to measure the *wefb* of the systems that contain the reactants in order to control the synthesis of nanoparticles. One of the challenges in the preparation of nanoparticles via microemulsions is that the size of the water droplets containing the metal precursor(s) and the reducing agent, respectively, should be the same. It is only under these conditions that an important open question, namely the relation between templating droplet and final particle size, can be studied systematically. Hence the aim of our work was to investigate the relevant phase diagrams of

[2] Once the conditions for co-reducing the two metal salts have been found, it should be possible to tune the composition of the nano-alloy via the composition of μe1.

microemulsions that contain metal precursor(s) (μe1) and reducing agent (μe2), respectively, which will be used for the synthesis of mono- and intermetallic nanoparticles in future studies. The challenge is to find the conditions under which the location of the *wefb*s of μe1 and μe2 are (nearly) the same and thus to be able to mix two microemulsions the water droplets of which have the same size and shape.

As was explained in the experimental section, the microemulsions under investigation consisted of an aqueous phase that contained metal salts ($H_2PtCl_6 \cdot 6H_2O$, $Bi(NO_3)_3 \cdot 5H_2O$, $Pb(NO_3)_2$, $H_2PtCl_6 \cdot 6H_2O$ + $Bi(NO_3)_3 \cdot 5H_2O$, $H_2PtCl_6 \cdot 6H_2O$ + $Pb(NO_3)_2$) or reducing agent ($NaBH_4$). In all of the experiments the surfactant to oil ratio (γ_b) was kept constant. We changed the composition of the aqueous phase and measured the phase diagram as a function of the content of the aqueous phase (w_A) and the co-surfactant (w_D), respectively. As described in section 3, the addition of the different salts led to a shift of the phase boundaries and thus of the *wefb*. The general influence of salt on the location of the *wefb* is known and can be explained qualitatively as follows: The salt ions compete with the counterions and the head groups for hydration water and thus decrease the hydrophilicity of the surfactant. In addition, the electrostatic repulsive interactions between the head groups decrease with increasing salt concentration and increasing ionic strength[3], respectively, which also reduces the area per head group and thus the curvature. Because of these two effects less 1-butanol is required to invert the curvature from positive (oil-in-water droplets) to negative (water-in-oil droplets) values, which, in turn, shifts the *wefb* to lower butanol contents with increasing salt concentration or increasing ionic strength. If the salt concentration and the ionic strength were the only tuning parameters it would be possible to formulate two microemulsions with equal *wefb*s simply by playing around with the type and amount of electrolyte. However, the results obtained for the Bi-salt as well as for the mixture of Pt- and Bi-salt cannot be explained either by different concentrations or by different ionic strengths. In order to gain more insight into the influence of salts on the location of the *wefb* we compared the results for various 1:1 electrolytes in more detail, which will be shown and discussed in the following.

The question to be answered is: "Are the molar concentration *c* and the ionic strength *I* the only relevant tuning parameters for the *wefb*?" If the answer was yes, phase diagrams measured at same *c* and *I* would be equal, which, in turn would allow us to adjust the location of the *wefb* simply by adding respective electrolytes. The results for the Bi-salt containing microemulsions, however, suggested a more complex answer. To clarify this point we measured phase diagrams of systems

[3] The ionic strength of the aqueous solution of an electrolyte can be calculated according to $I = 0.5 \sum_i z_i^n c_i$ where I is the ionic strength, z_i the charge, and c_i the concentration of each ion present in the solution.

containing different 1:1 electrolytes at the same *c* and *I* (note that *c* = *I* for 1:1 electrolytes). The resulting phase diagrams are shown in Fig.4 and in the Supporting Material Section. The compositions of the aqueous phases are given in Tab.3.

Figure 4

Table 3

As can be seen in Fig.4, the phase diagrams are far from being equal. A more detailed analysis reveals that all but one (see Supporting Material) of the shifts follow the concept of 'hard and soft acids and bases' (HSAB concept) [48,49]. Based on this order one can argue that the harder the acid (base) for a given base (acid) the more hydrated the ions, which, in turn, shifts the *wefb* to lower 1-butanol and water contents. This is exactly what is seen in Fig.4. Comparing Fig.4(a) and (b) one sees the influence of the anion: For a given cation the *wefb* of the Cl^- containing microemulsion is shifted downwards as Cl^- is a stronger base than NO_3^-. The same holds true for the influence of the cation: For a given anion the *wefb* of the H^+ containing microemulsion is shifted downwards as H^+ is a stronger acid than Na^+ (see also Supporting Material, Fig.S3).

We like to conclude this chapter by looking once again at the results obtained for the Bi-salt (Fig.2(b) and Fig.3(a)). As discussed above, the shift of the phase boundaries cannot be explained by different molar concentrations or ionic strengths. However, the HSAB concept allows us to understand the experimental observation. The microemulsions containing Bi-salt also contain a huge amount of HNO_3. In the corresponding reducing microemulsion this huge amount of electrolyte was compensated for by adding $NaNO_3$. Thus the main cation in μe1 is H^+, while it is Na^+ in μe2. The harder acid H^+ is more strongly hydrated than Na^+, which, in turn, shifts the *wefb* towards lower 1-butanol contents as explained above.

5. Conclusion and Outlook

For the planned synthesis of metallic Pt, Pb, and Bi nanoparticles via microemulsions the base system H_2O/salt – *n*-decane – SDS – 1-butanol and the metal salts H_2PtCl_6, $(PbNO_3)_2$, and $Bi(NO_3)_3$ have been chosen. $NaBH_4$ was used as reducing agent. To understand how the size and structure of the resulting nanoparticles depend on the size and structure of the microemulsion, studying the phase behaviour of the microemulsion is of prime importance. For example, the location of the water emulsification failure boundary (*wefb*) tells us under which conditions spherical water-in-oil droplets are formed. Although this is most often overlooked and nanoparticles

can indeed be synthesized without knowing the *wefb*, we are convinced that it is only via phase diagrams that we can understand the correlation – if any – between droplet size of the microemulsion and the size and shape of the resulting nanoparticles. Thus our approach is to mix μe1 (metal salt containing microemulsion) and μe2 (reducing agent containing microemulsion) only if the water droplets have the same size and shape, *i.e.* to measure the *wefb* of both microemulsions. The challenge is to find those conditions under which μe1 and μe2 have the same *wefb*, *i.e.* the tuning parameters for the location of the *wefb*. Different *wefb*s were obtained for different amounts and types of salt. As expected, the higher the molar concentration *c* and the larger the ionic strength *I*, the larger the shift of the phase boundaries towards lower 1-butanol contents. However, this general trend was not reflected in the results we obtained for microemulsions containing Bi-salt, which prompted us to have a closer look at the type of salt. We found that even at constant *c* and *I* the location of the *wefb* was different for different salts. The shift of the *wefb* could be explained with the HSAB concept: the harder the acid and the harder the base, the more hydrated the ion, which, in turn, shifts the *wefb* towards lower 1-butanol contents.

In conclusion, the tuning parameters for the location of the *wefb* are (a) the molar concentration *c* of the electrolyte, (b) the ionic strength *I* of the system, and (c) the hardness of the acid and base, respectively. Obviously these three parameters are interrelated in a complicated way and they have to be adjusted such that the average hydration of the surfactant in μe1 and μe2 is the same. Based on the presented results we suggest the following recipe to obtain equal *wefb*s: start with two microemulsions such that both have the same ionic strength and then fine-tune the location of the *wefb* by replacing some of the electrolyte. If you want to shift the *wefb* of one system upwards, use a salt that consists of a weaker acid and/or a weaker base. If you want to shift the *wefb* of one system downwards, use a salt that consists of a stronger acid and/or a stronger base. We will follow this recipe in our future work. The resulting phase diagrams will then form the basis for the synthesis of nanoparticles. The final aim is to understand the relation between the size of the microemulsion droplet and the size and shape, respectively, of the resulting nanoparticles.

Acknowledgment

R.N. would like to thank UCD Center for Synthesis and Chemical Biology (CSCB) for financial support. The authors thank Mrs. Andrea Kelly for measuring two of the phase diagrams during her final year project. We are very thankful for illuminating discussions with R. Strey and T. Sottmann.

Figure captions

Figure 1: Phase diagrams of the base system: H_2O/NaCl – *n*-decane – SDS – 1-butanol, measured at 21°C and $\gamma_b = 0.05$, and at two different salt concentrations, namely $\varepsilon = 0.01$ and 0.02.

Figure 2: Phase diagrams of microemulsions containing one metal precursor measured at 21°C and $\gamma_b = 0.05$. (a) H_2O/H_2PtCl_6/NaCl – *n*-decane – SDS – 1-butanol; (b) $H_2O/Bi(NO_3)_3/HNO_3$ – *n*-decane – SDS –1-butanol; (c) $H_2O/Pb(NO_3)_2/NaNO_3$ – *n*-decane – SDS – 1-butanol. For the sake of comparison the phase diagrams of the corresponding reducing microemulsions are also shown (open symbols).

Figure 3: Phase diagrams of microemulsions containing two metal precursors measured at 21°C and $\gamma_b = 0.05$. (a) $H_2O/H_2PtCl_6/Bi(NO_3)_3/HNO_3$ – *n*-decane – SDS – 1-butanol; (b) H_2O/H_2PtCl_6/ $Pb(NO_3)_2/NaNO_3$ – *n*-decane – SDS – 1-butanol. For the sake of comparison the phase diagrams of the corresponding reducing microemulsions are also shown (open symbols).

Figure 4: Phase diagrams of H_2O/electrolyte – *n*-decane – SDS – 1-butanol microemulsions with different 1:1 electrolytes measured at 21°C and $\gamma_b = 0.05$. In all cases the weight fractions of the electrolytes were chosen such that the molar concentration and thus the ionic strength of the aqueous phase was the same (see Tab. 3). We tested the effect of the anion in the presence of Na^+ (a) and H^+ (b) as counterion.

References

[1] S. Biallozor, A. Kupniewska, V. Jasulaitene, Fuel Cells 3 (2003) 8.

[2] H. Wang, T. Loffler, H. Baltuschat, J. Appl. Electrochem. 31 (2001) 759.

[3] M.M.P. Janssen, J. Moolhuysen, Electrochim. Acta 21 (1976) 361.

[4] T. Frelink, W. Wisscher, J.A.R. van Veen, Surf. Sci. 335 (1995) 353.

[5] M.-Sh. Liao, C.R. Carbrera, Y. Ishikawa, Surf. Sci. 445 (2000) 267.

[6] H. Massong, H. Wang, G. Samjeske, H. Baltruschat, Electrochim. Acta 46 (2000) 701.

[7] A. Kelaidoupolou, E. Abelidou, A. Papoutsis, E.K. Polychroniadis, G. Kokkinidis, J. Appl. Electrochem. 28 (1998) 1101.

[8] S. Swathirajan, Y.M. Mikhail, J. Electrochem. Soc. 139 (1992) 2105.

[9] C. Lamy, E.M. Belgsir, J.-M. Leger, J. Appl. Electrochem. 31 (2001) 799.

[10] V.S. Bagotzky, L.A. Kanevsky, V.Sh. Palanker, Electrochim. Acta 18 (1973) 473.

[11] K. Wang, H.A. Gasteiger, N.M. Markovic, P.N. Ross jr, Electrochim. Acta 41 (1996) 2587.

[12] A.N. Haner, P.N. Ross, J. Phys. Chem. 95 (1991) 3740.

[13] N. Furaya, S. Motoo, J. Electroanal. Chem. 99 (1979) 195.

[14] Y. Ishikawa, M.-S. Liao, C.R. Carbera, Surf. Sci. 463 (2000) 66.

[15] M. Kubota, Inorg. Chem. 29 (1990) 574.

[16] A.P. Alivisatos, Science 271 (1996) 933.

[17] J. Chen, T. Herricks, M. Geissler, Y. Xia, J Am. Chem. Soc. 126 (2004) 10854.

[18] M.P. Pileni, Langmuir 17 (2001) 7476.

[19] S. Komarneni, D. Li, B. Newalkar, H. Katsuki, A.S. Bhalla, Langmuir 18 (2002) 5959.

[20] D. Volpe, E. Casado-Rivera, L. Alden, C. Lind, K. Hagerdon, C. Downie, C. Korzeniewski, F.J. DiSalvo, H.D. Abruna, J. Electrochem. Soc. 151 (2004) A971.

[21] E. Casado-Rivera, D. Volpe, L. Alden, C. Lind, C. Downie, T. Vazquez-Alvarez, A.C.D. Angelo, F.J. DiSalvo, H.D. Abruna, J. Am. Chem. Soc. 126 (2004) 4043.

[22] C. Roychowdhury, F. Matsumoto, V.B. Zeldovich, S.C. Warren, P.F. Mutolo, M.J. Ballesteros, U. Wiesner, H.D. Abruña, F.J. DiSalvo, Chem. Mater. 18 (2006) 3365.

[23] L.R. Alden, C. Roychowdhury, F. Matsumoto, D. Han, V. B. Zeldovich, H.D. Abruña, F.J. DiSalvo, Langmuir 22 (2006) 10465.

[24] C. Roychowdhury, F. Matsumoto, P.F. Mutolo, H.D. Abruña, F.J. DiSalvo, Chem. Mater. 17 (2005) 5871.

[25] L.R. Alden, D. Han, F. Matsumoto, H.D. Abruña, F.J. DiSalvo, Chem. Mater. 18 (2006) 5591.

[26] I. Capek, Adv. Colloid Interface Sci. 110 (2004) 49.

[27] V. Uskoković, M. Drofenik, Surf. Rev. Lett. 12 (2005) 239.
[28] C. Stubenrauch, T. Wielpütz, T. Sottmann, C. Roychowdhury, F.J. DiSalvo, Colloids and Surfaces A 317 (2008) 328.
[29] C. Stubenrauch, PhD Thesis, Technical University Berlin, 1997.
[30] T. Sottmann, R. Strey in: J. Lyklema (Ed.), Soft Colloids V – Fundamentals in Interface and Colloid Science, Elsevier, Amsterdam, 2005, chapter 5.
[31] M.L. Wu, L.B. Lai, Colloids and Surfaces A 244 (2004) 149.
[32] M.L. Wu, D.H. Chen, T.C. Huang, Chem. Mater. 13 (2001) 599.
[33] M.L. Wu, D.H. Chen, T.C. Huang, J. Colloid Interface Sci. 243 (2001) 102.
[34] B.J. Hwang, Y.W. Tsai, L.S. Sarma, Y.L. Tseng, D. G.Liu, J.F. Lee, J. Phys. Chem. B, 108 (2004) 20427.
[35] R. Strey, Colloid Polym. Sci. 272 (1994) 1005.
[36] T. Hellweg, A. Brûlet, T. Sottmann, PCCP 2 (2000) 5168.
[37] M. Gradzielski, D. Langevin, T. Sottmann, and R. Strey, J. Chem. Phys. 106 (1997) 8232.
[38] M. Gradzielski, D. Langevin, B. Farago, Phys. Rev. E 53 (1996) 3900.
[39] U. Olsson, and P. Schurtenberger, Langmuir 9 (1993) 3389.
[40] K. Kluge, C. Stubenrauch, T. Sottmann, and R. Strey, Tenside Surf. Det. 38 (2001) 30.
[41] L. Belkoura, C. Stubenrauch, and R. Strey, Langmuir 20 (2004) 4391.
[42] T. Sottmann, Bunsen Magazin 6 (2006) 163.
[43] A. Bumajdad, J. Eastoe, M.I. Zaki, R.K. Heenan, L. Pasupulrty, J. Colloid Interface Sci. 312 (2007) 68.
[44] M. Kahlweit, R. Strey, J. Phys. Chem. 92 (1988) 1557.
[45] M. Kahlweit, R. Strey, P. Firman, J. Phys. Chem. 90 (1986) 671.
[46] M. Kahlweit, G. Busse, B. Faulhaber, Langmuir 10 (1994) 1134.
[47] H. Kunieda, J. Colloid Interface Sci. 122 (1988) 138.
[48] R.G. Pearson, Surv. Prog. Chem. 5 (1969) 1.
[49] M. Kahlweit, R. Strey, P. Firman, D. Haase, J. Jen, R. Schomäcker, Langmuir 4 (1988) 499.
[50] J.L. Kurz, J. Phys. Chem. 66 (1962) 2239.

Figure captions

Figure 1: Phase diagrams of the base system: H_2O/NaCl – *n*-decane – SDS – 1-butanol, measured at 21°C and γ_b = 0.05, and at two different salt concentrations, namely ε = 0.01 and 0.02.

Figure 2: Phase diagrams of microemulsions containing one metal precursor measured at 21°C and γ_b = 0.05. (a) H_2O/H_2PtCl_6/NaCl – *n*-decane – SDS – 1-butanol; (b) $H_2O/Bi(NO_3)_3/HNO_3$ – *n*-decane – SDS –1-butanol; (c) $H_2O/Pb(NO_3)_2/NaNO_3$ – *n*-decane – SDS – 1-butanol. For the sake of comparison the phase diagrams of the corresponding reducing microemulsions are also shown (open symbols).

Figure 3: Phase diagrams of microemulsions containing two metal precursors measured at 21°C and γ_b = 0.05. (a) $H_2O/H_2PtCl_6/Bi(NO_3)_3/HNO_3$ – *n*-decane – SDS – 1-butanol; (b) H_2O/H_2PtCl_6/ $Pb(NO_3)_2/NaNO_3$ – *n*-decane – SDS – 1-butanol. For the sake of comparison the phase diagrams of the corresponding reducing microemulsions are also shown (open symbols).

Figure 4: Phase diagrams of H_2O/electrolyte – *n*-decane – SDS – 1-butanol microemulsions with different 1:1 electrolytes measured at 21°C and γ_b = 0.05. In all cases the weight fractions of the electrolytes were chosen such that the molar concentration and thus the ionic strength of the aqueous phase was the same (see Tab. 3). We tested the effect of the anion in the presence of Na^+ (a) and H^+ (b) as counterion.

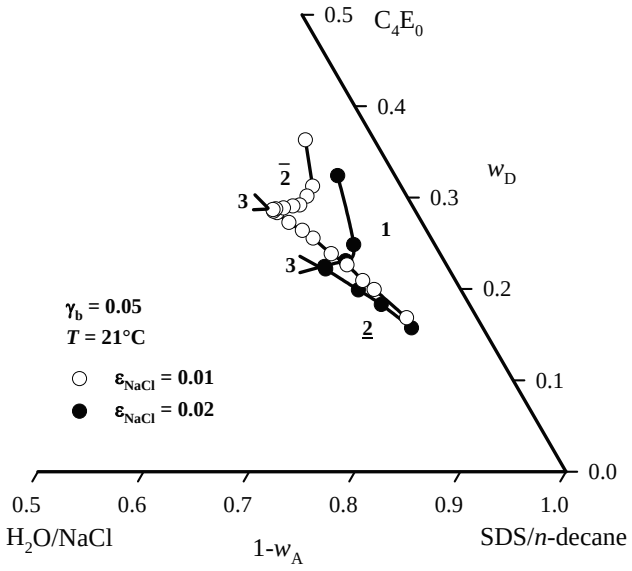

Figure 1: Najjar et al.

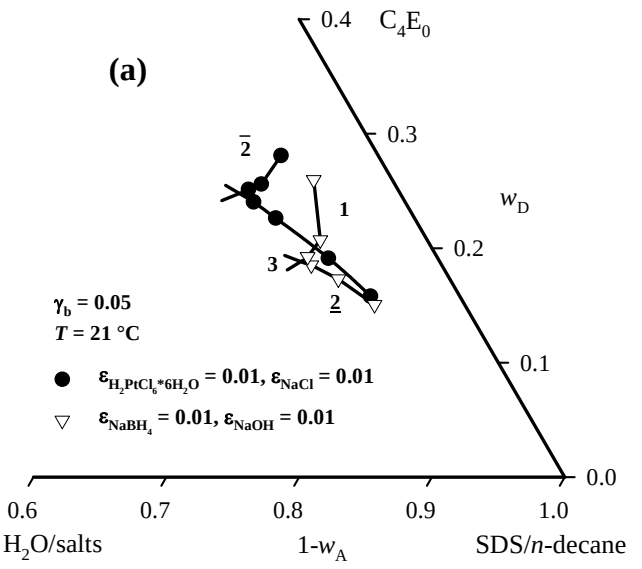

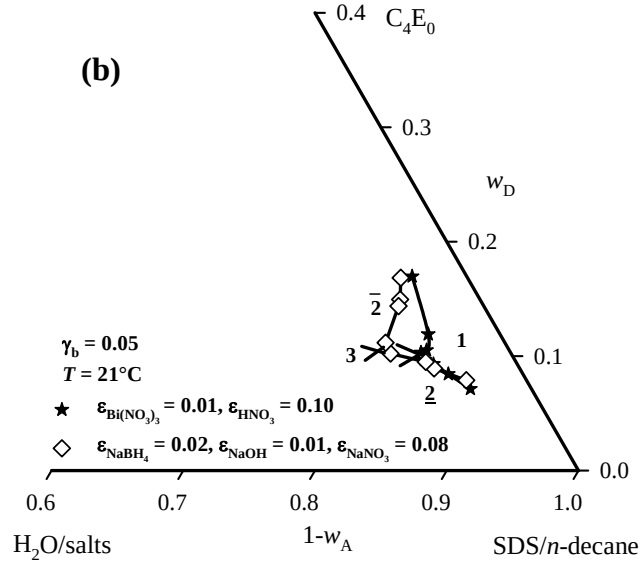

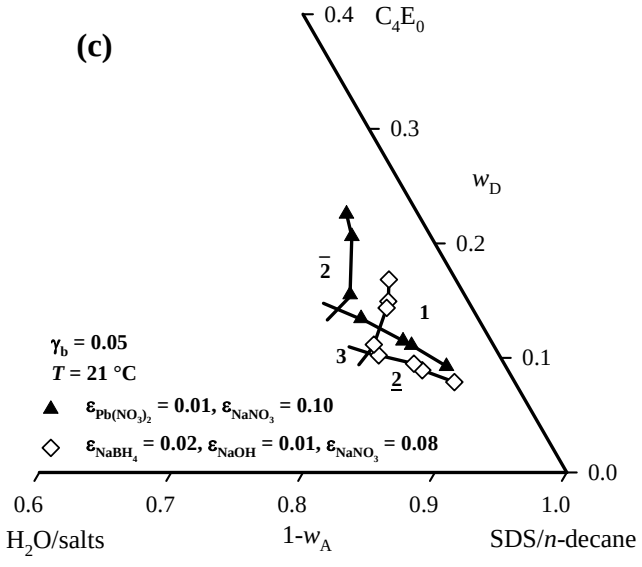

Figure 2: Najjar et al.

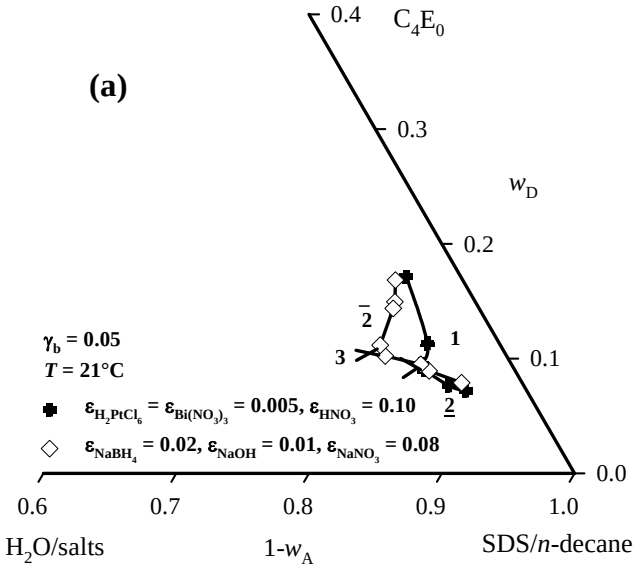

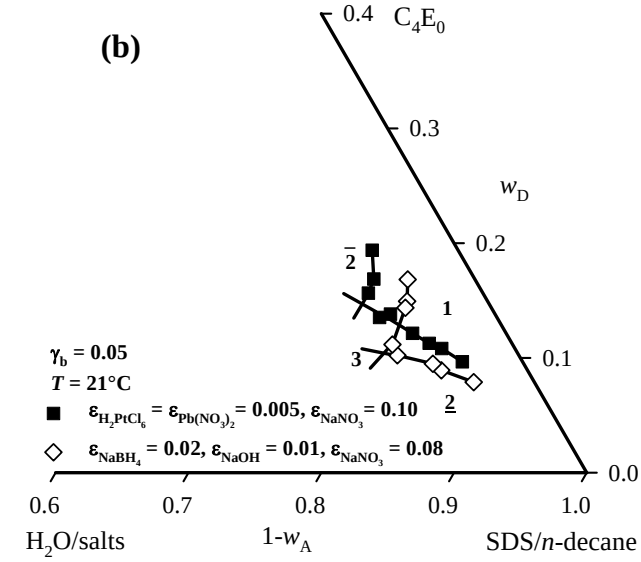

Figure 3: Najjar et al.

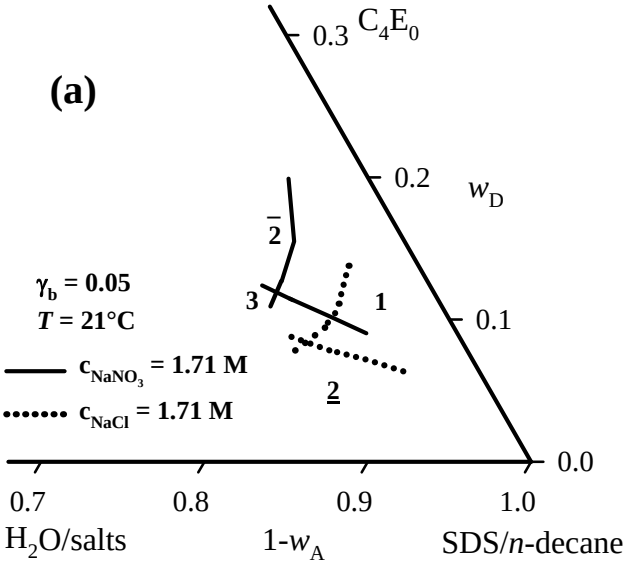

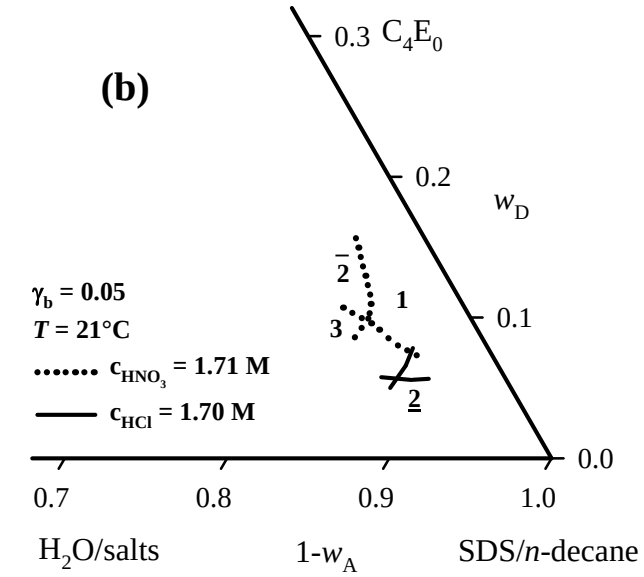

Figure 4: Najjar et al.

Table 1: Composition of aqueous phases containing the reducing agent $NaBH_4$ given in weight fractions ε (and in concentrations *c* / M); *I* is the ionic strength of the aqueous phases. Phase diagrams are shown in the indicated Figures.

Phase Diagram	ε (*c* / M) $NaBH_4$	ε (*c* / M) NaOH	ε (*c* / M) $NaNO_3$	ε (*c* / M) total	*I* / M
Fig.S2(a)	0.01 (0.26)	0.01 (0.25)	-	0.02 (0.51)	0.51
Fig.S2(a)	0.02 (0.52)	0.01 (0.25)	-	0.03 (0.77)	0.77
Fig.S2(b)	0.02 (0.52)	0.01 (0.25)	0.08 (0.94)	0.11 (1.71)	1.71

Table 2: Composition of aqueous phases containing the metal precursor(s) given in weight fractions ε (and in concentrations *c* / M); *I* is the ionic strength of the aqueous phases. Phase diagrams are shown in the indicated Figures.

Phase Diagram	metal salt(s)	ε (*c* / M) metal salt	ε (*c* / M) electrolyte	ε (*c* / M) total	*I* / M
Fig.2(a)	H_2PtCl_6	0.01 (0.02)	0.01 (0.17) NaCl	0.02 (0.19)	0.23
Fig.2(b)	$Bi(NO_3)_3$	0.01 (0.02)	0.10 (1.59) HNO_3	0.11 (1.61)	1.71
Fig.2(c)	$Pb(NO_3)_2$	0.01 (0.03)	0.10 (1.18) $NaNO_3$	0.11 (1.21)	1.27
Fig.3(a)	H_2PtCl_6 $Bi(NO_3)_3$	0.005 (0.01) 0.005 (0.01)	0.10 (1.59) HNO_3	0.11 (1.61)	1.68
Fig.3(b)	H_2PtCl_6 $Pb(NO_3)_2$	0.005 (0.01) 0.005 (0.015)	0.10 (1.18) $NaNO_3$	0.11 (1.205)	1.26

Table 3: Weight fractions ε, concentrations *c*, and ionic strength *I* of the aqueous phases which were used to study the effect of the different electrolytes on the phase diagrams of the microemulsion H_2O/salts – *n*-decane – SDS – 1-butanol.

electrolyte	ε	*c* / M	*I* / M
NaCl	0.100	1.71	1.71
NaOH	0.068	1.70	1.70
$NaNO_3$	0.145	1.71	1.71
HNO_3	0.108	1.71	1.71
HCl	0.062	1.70	1.70

S1 Phase Diagrams of the Base Microemulsion System

As can be seen in Fig.1 and Fig.S1, the NaOH and the NaCl system show a “funnel shaped” phase diagram with the wide side of the funnel directed towards high oil/surfactant contents. The “interior” of the funnel indicates the compositions of the system at which a one-phase microemulsion (1) is observed. At 1-butanol contents below the lower phase boundary an oil-in-water (o/w) microemulsion coexists with an oil excess phase (2), while at 1-butanol contents above the upper phase boundary a w/o-microemulsion coexists with a water excess phase ($\bar{2}$). It is this upper phase boundary between 1 and $\bar{2}$ that is called the *wefb* and which needs to be determined to know under which conditions spherical water droplets in a continuous oil phase are formed. Increasing the content of the aqueous phase (*i.e.* increasing w_A) along the *wefb* one obtains water droplets of increasing size until the three-phase region is reached (3) where a bicontinuous microemulsion coexists with an oil and an aqueous excess phase. In other words, knowing the location of the *wefb* one can control both the shape and the size of the microemulsion droplets.

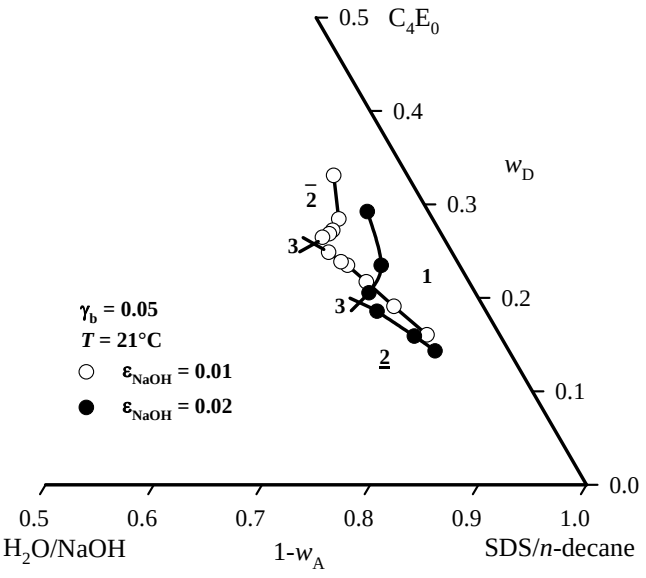

Fig. S1: Phase diagrams of the base system H_2O/NaOH – *n*-decane – SDS – 1-butanol measured at 21°C, γ_b = 0.05 and at two different salt concentrations, namely ε = 0.01 and 0.02.

S2 Phase Diagrams of Microemulsions containing Reducing Agent

As was the case for the systems seen in Fig.1 and Fig.S1, the location of the *wefb* is affected if one changes the total salt content. Comparing Fig.S1with Fig.S2(a) one sees that the *wefb* at ε_{total} = 0.03 is again shifted towards lower water and 1-butanol contents compared to those measured at ε_{total} = 0.01 and 0.02, respectively. As was the case for NaOH and NaCl, the *wefb* at equal ε-values (ε_{NaOH} = 0.02 in Fig.S1 compared to ε_{NaBH4} + ε_{NaOH} = 0.02 in Fig.S2(a)) is also slightly affected. The difference, however, is very small as the molecular weights and thus the molar concentrations of $NaBH_4$ and NaOH are nearly the same (see Tab.1). Looking at Fig.S2(b) one sees that the shift towards lower water and 1-butanol contents is more pronounced due to the larger electrolyte content (ε_{total} = 0.11). As was the case for NaOH and NaCl, the *wefb* at equal ε-values (ε_{NaOH} = 0.02 in Fig.S1 compared to ε_{NaBH4} + ε_{NaOH} = 0.02 in Fig.S2(a)) is also slightly affected. The difference, however, is very small as the molecular weights and thus the molar concentrations of $NaBH_4$ and NaOH are nearly the same (see Tab.1). Looking at Fig.S2(b) one sees that the shift towards lower water and 1-butanol contents is more pronounced due to the larger electrolyte content (ε_{total} = 0.11). An observation worthwhile mentioning is the fact that an increase from ε = 0.01 to 0.02 (Fig. 1) has a larger effect on the *wefb* than an increase from ε = 0.03 to 0.11 (see supporting Material, Fig. S2).

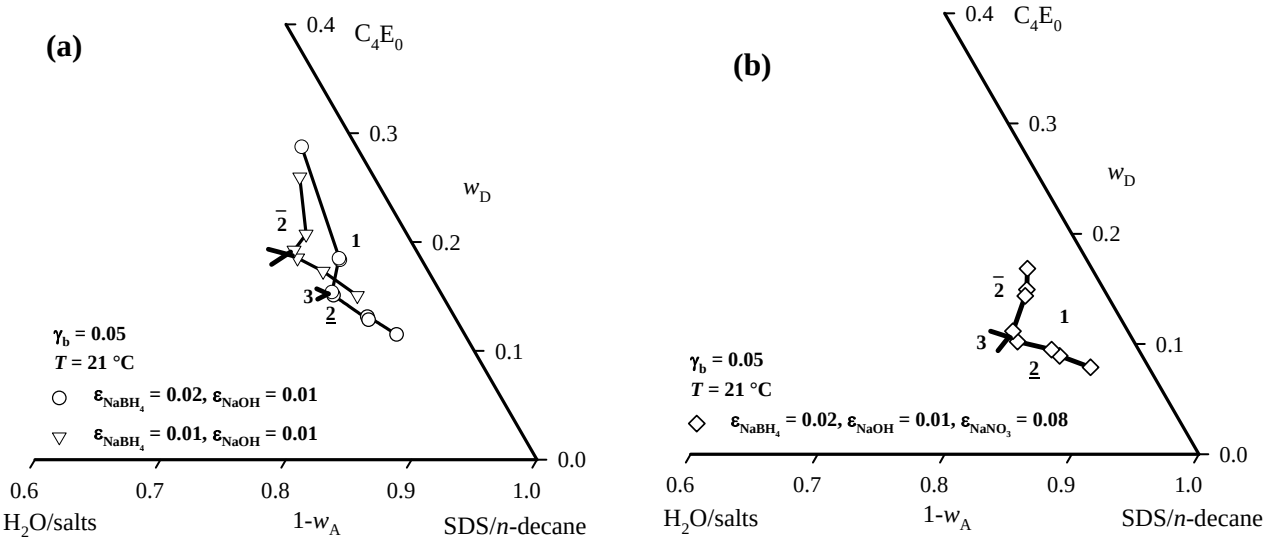

Fig. S2: Phase diagrams of microemulsions containing the reducing agent measured at 21°C and γ_b = 0.05. (a) $H_2O/NaBH_4/NaOH$ – *n*-decane – SDS – 1-butanol at two different amounts of $NaBH_4$; (b) $H_2O/NaBH_4/NaOH/NaNO_3$ – *n*-decane – SDS – 1-butanol.

S3 Phase Diagrams of Microemulsions and the HSAB concept

According to the concept of 'hard and soft acids and bases' (HSAB concept), 'hard' applies to species which are small, have high charges (the charge criterion applies mainly to acids, to a lesser extent also to bases), and are weakly polarizable. 'Soft' applies to species which are big, have low charges and are strongly polarizable. The harder a base and an acid, respectively, the more hydrated it is. For the ions of the present study the following order holds (decreasing strength):

(a) Acids: $H^+ > Na^+ > Pt^{4+} > Bi^{3+} > Pb^{2+}$

(b) Bases: $OH^- > Cl^- > NO_3^- > BH_4^- > PtCl_6^{2-}$

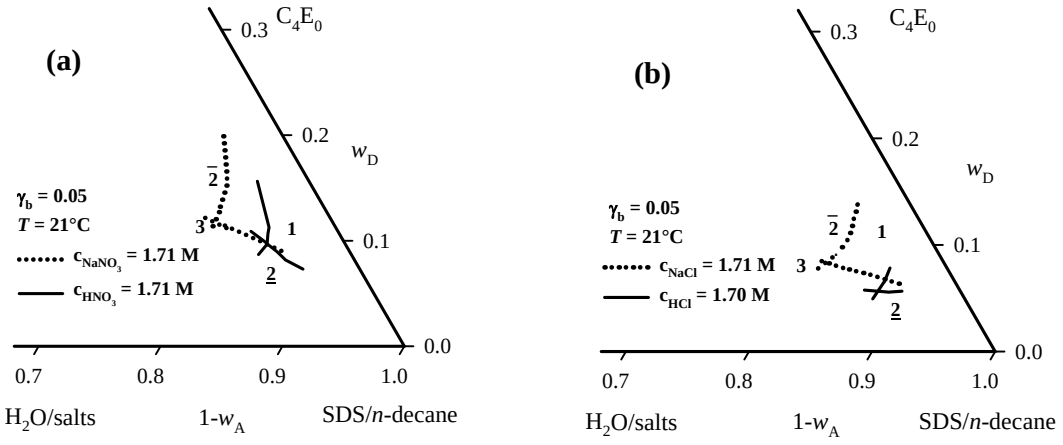

Fig. S3: Phase diagrams of H_2O/electrolyte – *n*-decane – SDS – 1-butanol microemulsions with different 1:1 electrolytes measured at 21°C and $\gamma_b = 0.05$. In all cases the weight fractions of the electrolytes were chosen such that the molar concentration and thus the ionic strength of the aqueous phase was the same (see Tab. 3). We tested the effect of the cation in the presence of NO_3^- (a) and Cl^- (b) as counterion.

As mentioned in Section 4 all but one of the *wefb* shifts follow the concept of 'hard and soft acids and bases' (HSAB concept). The exception is seen in Fig.S4, where phase diagrams of NaCl, NaOH, and $NaNO_3$ at same ionic strengths are shown.

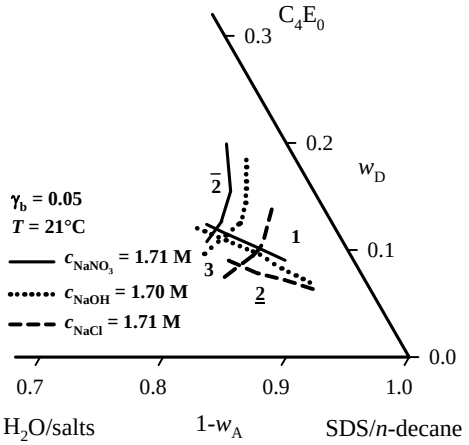

Figure S4: Phase diagrams of H_2O/electrolyte – *n*-decane – SDS – 1-butanol microemulsions with different 1:1 electrolytes measured at 21°C and γ_b = 0.05. In all cases the weight fractions of the electrolytes were chosen such that the molar concentration and thus the ionic strength of the aqueous phase was the same (see Tab. 3). We tested the effect of the anion in the presence of Na^+ as counterion.

According to the HSAB concept the strength of the base decreases in the following order: $OH^- > Cl^- > NO_3^-$, which, in turn, should lead to a shift of the *wefb* towards lower 1-butanol contents from $NO_3^- > Cl^- > OH^-$. As can be seen in Fig.S4 this is not the case. Note that two of the systems are neutral solutions, while one is a base solution. One possible explanation for this observation may be different degrees of SDS hydrolysis in the neutral compared to the base solution. Note that SDS is relatively stable in neutral and basic solution but undergoes hydrolysis in acidic solutions or in neutral solutions at elevated temperatures [50]. Although we did not store the solutions but always prepared new ones we cannot exclude some hydrolysis of the surfactant. Different degrees of hydrolysis in the neutral (NaCl, $NaNO_3$) and the base (NaOH) solutions would lead to a shift of the phase boundaries. The hydrolysis would lead to a decrease of the SDS concentration and the production of surface-active dodecanol. Dodecanol would render the oil phase less hydrophobic and the interface more hydrophobic, which, in turn, would shift the *wefb* downwards. As speculative it may be, one could explain the trend in Fig.S4 by a strong hydrolysis of SDS in the NaCl containing μe. The produced dodecanol causes an additional shift of the *wefb* to lower 1-butanol contents.